

Since January 2020 Elsevier has created a COVID-19 resource centre with free information in English and Mandarin on the novel coronavirus COVID-19. The COVID-19 resource centre is hosted on Elsevier Connect, the company's public news and information website.

Elsevier hereby grants permission to make all its COVID-19-related research that is available on the COVID-19 resource centre - including this research content - immediately available in PubMed Central and other publicly funded repositories, such as the WHO COVID database with rights for unrestricted research re-use and analyses in any form or by any means with acknowledgement of the original source. These permissions are granted for free by Elsevier for as long as the COVID-19 resource centre remains active.

Energy & Buildings 278 (2023) 112623

Contents lists available at ScienceDirect

Energy & Buildings

journal homepage: www.elsevier.com/locate/enb

Analysis on the thermal performance of low-temperature radiant floor coupled with intermittent stratum ventilation (LTR-ISV) for space heating

Xiangfei Kong [a], Yufan Chang [a,b], Man Fan [a], Han Li [a,*]

[a] School of Energy and Environmental Engineering, Hebei University of Technology, Tianjin 300401, China
[b] Department of Building Environment and Energy, College of Civil Engineering, Hunan University, Changsha 410082, China

ARTICLE INFO

Article history:
Received 18 July 2022
Revised 7 October 2022
Accepted 28 October 2022
Available online 3 November 2022

Keywords:
LTR-ISV
Thermal comfort
Airborne transmission risk
Energy and exergy efficiency
Space heating

ABSTRACT

With increasing energy use and outbreaks of respiratory infectious diseases (such as COVID-19) in buildings, there is a growing interest in creating healthy and energy-efficient indoor environments. A novel heating system named low-temperature radiant floor coupled with intermittent stratum ventilation (LTR-ISV) is proposed in this study. Thermal performance, indoor air quality, energy and exergy performance were investigated and compared with conventional radiant floor heating (CRFH) and conventional radiant floor heating with mixing ventilation (CRFH + MV). The results indicated that LTR-ISV had a more uniform operative temperature distribution and overall thermal sensation, and air mixing was enhanced without generating additional draft sensation. Compared with CRFH and CRFH + MV, the indoor CO_2 concentration in LTR-ISV can be reduced by 1355 ppm and 400 ppm, respectively. Airborne transmission risk can also be reduced by 5.35 times. The coefficient of performance for CRFH, CRFH + MV, and LTR-ISV during working hours was 4.2, 2.5, and 3.4, respectively. The lower value of LTR-ISV was due to the high energy usage of the primary air handing unit. In the non-working hours, LTR-ISV was 0.6 and 1.3 higher compared to CRFH and CRFH + MV, respectively. The exergy efficiency of LTR-ISV, CRFH, and CRFH + MV was 81.77 %, 76.43 %, and 64.71 %, respectively. Therefore, the LTR-ISV system can meet the requirements of high indoor air quality and thermal comfort and provides a reference for the energy-saving use of low-grade energy in space heating.

© 2022 Elsevier B.V. All rights reserved.

1. Introduction

With the heating network exceeding 200,000 km [1], China now has the longest district heating system in the world, and such a long network leads to a large amount of energy use. In 2020, space heating took up 20 % of China's building energy use [2]. Accordingly, China's heating system consumes mainly coal, accounting for 84 % of the total consumption [3]. In 2020 alone, the total consumption for space heating is 0.214 billion tons of standard coal, which is still increasing rapidly due to accelerated urbanization (from 5 billion square meters in 2001 to 15.6 billion square meters in 2020) [4]. Large combustion of coal results in high concentrations of SO_2, NO_x, and CO_2 in the outdoor environment [5,6], which are key factors contributing to hazy weather [7]. Worse still, outdoor pollutants can easily enter indoors through the gaps of the building, resulting in poor indoor air quality [8]. Long-term exposure to poor indoor environments can lead to the development of diseases such as sick building syndrome and building-related illness [9]. All these problems will seriously affect the health of indoor occupants.

Besides, epidemic prevention and control have become a new focus of attention now. Since 2020, a novel pneumonia pandemic called COVID-19, caused by SARS-CoV-2, has rapidly spread to more than 200 countries. By July 11th, 2022, 552,502,629 cases were confirmed including 6,347,816 deaths [10]. There are three main transmission routes, namely contact transmission, droplet transmission [11,12], and aerosol transmission [13]. The former two routes can be coped by appropriate surface cleaning and hand hygiene, and keeping social distance [14] and wearing masks [15], respectively. The transmission through aerosols in indoor environments is primarily caused by poor ventilation [16]. Therefore improving ventilation is considered as an efficient solution to reduce airborne transmission risk such as increasing ventilation rates [17] and using advanced airflow organization [18]. Those findings have triggered numerous investigations to the creation

* Corresponding author.
E-mail address: lihan18113@hebut.edu.cn (H. Li).

https://doi.org/10.1016/j.enbuild.2022.112623
0378-7788/© 2022 Elsevier B.V. All rights reserved.

Nomenclature

A	Area (m^2)
c	Contaminant concentration (ppm)
c_p	Air specific heat (kJ/kg·K)
E_Z	Zone air distribution effectiveness
e_p^c	Local relative contaminant exposure index
ex	Exergy (kW)
G	Fresh air volume (kg/s)
h	Enthalpy (kJ/kg)
h_r	Radiative heat-transfer coefficient ($W/m^2 \cdot ^oC$)
h_c	Convective heat-transfer coefficient ($W/m^2 \cdot ^oC$)
I	Numbers of infector
k_a	Air conductive heat transfer coefficient at supply air temperature ($W/m \cdot ^oC$)
L	Characteristic length (m)
Nu	Nusselt number
p	Pulmonary ventilation rate (m^3/h)
P	Pressure (Pa)
P_I	Predicted infection risk (%)
P_r	Prandtl Number
q	Quantum generation rate (quantum/s)
Q	Heat supply (W)
R	Ideal gas constant (kg/kg·K)
Re	Reynolds number
T	Temperature (K)
t	Time (s)
T_N	Indoor air design temperature (^{o}C)
T_o	Operative temperature (^{o}C)
T_p	Area-weighted average temperature of the non-heated walls (^{o}C)
$\bar{T}_r$	Mean radiant temperature (^{o}C)
Tu	Turbulence intensity (%)
v	Air velocity (m/s)
$\bar{v}$	Average velocity (m/s)
V	Ventilation rate (m^3/s)
w	Humidity ratio (kg/kg dry air)
W	Power (W)

Greek symbols

η	Exergy efficiency (%)
ρ	Density (kg/m^3)
μ	Dynamic viscosity (Pa·s)
σ	Measurement uncertainty related to the repetition of the experiments

Abbreviations

ACH	Air changes per hour
AHU	air handing unit
ASHP	Air-source heat pump
COP	Coefficient of performance
CRFH	Conventional radiant floor heating
CRFH + MV	Conventional radiant floor heating + mixing ventilation
DR	The draft rate (%)
DOAS	Dedicated outdoor air system
LTR-ISV	Low-temperature radiant floor coupled with intermittent stratum ventilation
OTS	Overall thermal sensation
PAU	Primary air handing unit

Subscripts

0	Reference (environment) state
a	Indoor air
ch	Chemical
comp	Compressor
da	Dry air
e	Exhaust
fan	Mechanical ventilation fans
hc	Heating coil
in	Exergy input
loss	Exergy loss
me	Mechanical
out	Output
r	Radiant floor
s	Supply air
sd	Standard deviation
th	Thermal
v	Water vapor
wp	Water pump

of a healthy indoor air environment [19,20]. And the application of healthy and energy-efficient heating methods has also become an urgent concern.

In Northern China, where district heating is implemented, CRFH is widely used in buildings, which is achieved by embedding small water pipes into the concrete floor [21]. Compared to the 75 °C water supply temperature of radiators, the supply water temperature of CRFH can be reduced to 45 °C [22], thus allowing the use of low-grade energy as the heat source [23]. However, CRFH ignores the issue of indoor air quality. In regions with high concentrations of outdoor pollutants, the negative indoor pressure caused by the difference between indoor and outdoor air temperatures in winter can easily allow outdoor pollutants to enter the indoor environment. In recent years, for the concern of enhancing the energy efficiency of buildings, thermal insulation and air tightness of the envelope is getting better and better [24], which makes it difficult for outdoor pollutants to enter, but also impossible for indoor-generated pollutants to be expelled [25]. To enhance indoor air quality, radiant floor heating with fresh air supply has attracted considerable interest of researchers and has already been applied in practice [26], which is achieved by installing an additional mechanical ventilation system to send fresh air into the room, the volume of which is determined by the number of indoor occupants. However, this hybrid system has some drawbacks: (1) the fresh air volume is small and has limited improvement in indoor air quality; (2) mixing ventilation is less capable of removing indoor pollutants compared to other ventilation modes such as displacement ventilation [27]; (3) fresh air is heated to 1–3 °C below the indoor design temperature before being sent indoors [28], resulting in the fresh air that tends to sink and hardly stays at the occupied zone; and (4) the introduction of cold fresh air leads to an increase in fresh air load. Therefore, it is imperative to find a heating mode that can solve the above problems.

Stratum ventilation, which was proposed by Lin et al. [29] in 2005, is dedicated to providing thermal comfort [30,31] and good air quality [32] indoor environments with low energy use. Stratum ventilation delivers clean air via wall-mounted air inlets located on the sidewall at a height of 1.2 m. Compared to mixing ventilation, overall thermal sensation and overall thermal comfort are enhanced by 22.5 % and 10 %, respectively [33]. From an energy-saving point of view, the thermal neutral temperature of stratum ventilation is increased by 2.5 °C and 2.0 °C compared with dis-

placement ventilation and mixing ventilation, which can save 25.22 % and 44.37 % of primary energy in office applications in Hong Kong (Hot summer and warm winter climate), respectively [34]. In this context, this study coupled radiant floor heating and stratum ventilation into low-temperature radiant floor coupled with intermittent stratum ventilation (LTR-ISV) heating system. Unlike radiant floor, which is responsible for all the heat supply in CRFH and CRFH + MV, both radiant floor and stratum ventilation are responsible for part of the heat load in LTR-ISV. By applying this system, the surface temperature of radiant floor heating can be reduced to 24 °C, and the stratum ventilation with a low supply air temperature of 23 °C. The new system can enhance indoor air mixing and ensure a comfortable indoor environment with reduced energy use.

The selection of the heat source in the LTR-ISV system is a crucial factor influencing the system's performance. In this novel heating system, an air-source heat pump (ASHP) was selected as the heat resource for its high energy efficiency (COP above 2.25 [35] compared to 0.88–0.92 for coal- fired boilers [36]) and 46.6 % reduction in carbon emissions [37] compared with traditional coal-fired boilers. Regarding energy performance, previous studies normally analyzed energy use based on the first law of thermodynamics [38]. However, exergy analysis, which is based on the first and second law of thermodynamics, is of great significance due to that it reveals the irreversible entropy increase during the practical thermodynamic process and exergy loss [39], and provides solid evidence of energy efficiency and degradation [40]. Therefore, exergy analysis is an indispensable part of energy performance.

This study serves as a preliminary inquiry to the feasible use of the LTR-ISV heating system in cold climates. The focus is evaluating its performance on thermal environment, indoor air quality and energy efficiency compared to two conventional systems. The results can provide a reference for the energy-saving utilization of low-grade energy in space heating.

2. Methodology

The flowchart of this study is summarized in Fig. 1. the proposed system LTR-ISV was compared with CRFH and CRFH + MV through experiments and MATLAB simulations. The indoor thermal environment and air quality experiments were performed in an experimental room, where the results of airborne risk were obtained from experiments on indoor air quality. The energy performance results of the system are obtained by MATLAB simulations.

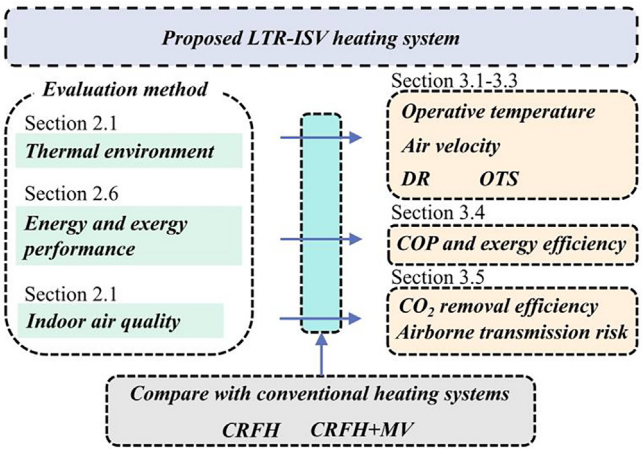


Fig. 1. Flowchart of the present study.

2.1. Experimental set-up

Indoor thermal environment was regulated by CRFH, CRFH + MV, and LTR-ISV (Fig. 2). An experimental room with the dimensions of 6 × 5.92 × 2.6 m (Length × Width × Height) was built to conduct the experiments. The room was located in Tianjin, which belongs to the cold climate zone of China, where the outdoor air temperature normally fluctuates between −5–0 °C. Fig. 3**(a)** shows the layout of the experimental room. The door was located on the south wall and two windows were located on the north wall. To prevent the heat of the radiant floor downward transfer, the thermal insulating layer and heat insulation layer were put beneath the heating layer, and covered with an insulation layer above to ensure uniform heat dissipation, the framework of which is shown in Fig. 4. For stratum ventilation settings, as shown in Fig. 3**(a)**, four air inlets (S1-S4) and four air outlets (S5-S8) were located on the east wall at the height of 1.2 m and 0.5 m, respectively, and the cross area of each air terminal was 0.04 m^2 (0.2 × 0.2 m). There are two 0.5 × 0.5 m ceiling-mounted mixing ventilation air inlets in the center of the ceiling and four outlets of the same size at the four corners, as shown in Fig. 3**(b)**. To maintain the stability of supply air temperature and velocity, a dry-bulb temperature sensor and a flow nozzle with the accuracy of ± 0.1 °C and ± 2 % were equipped.

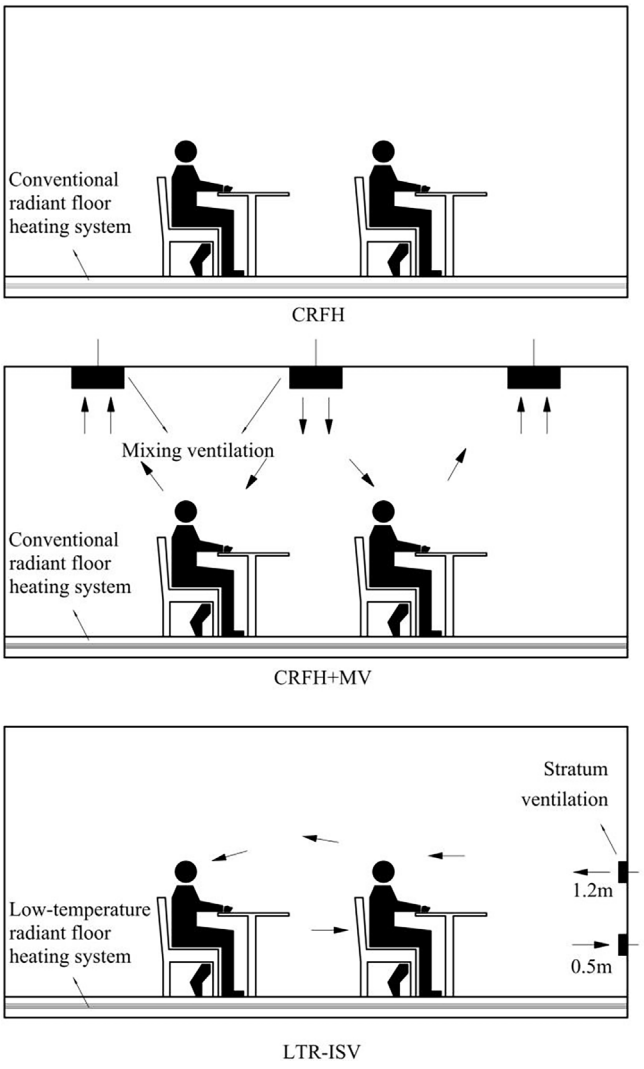


Fig. 2. Schematic diagram of the three heating modes.

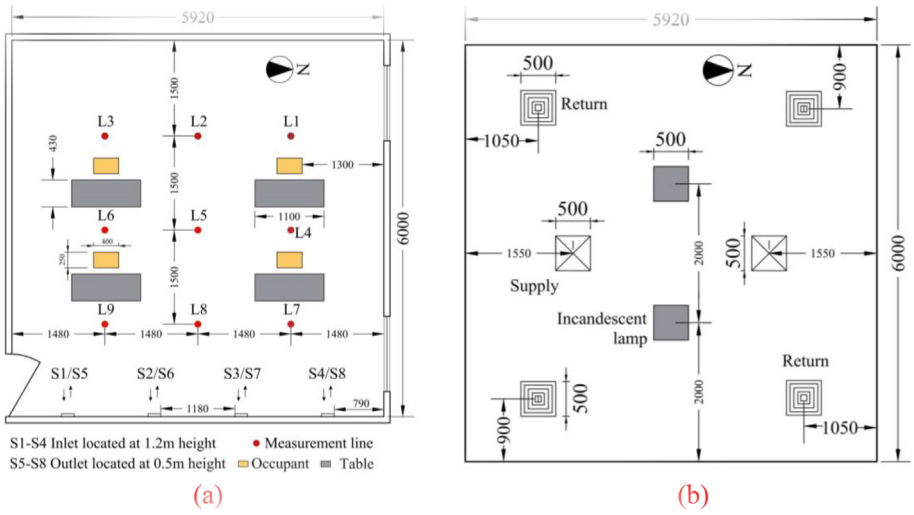


Fig. 3. Layout of the experimental room.

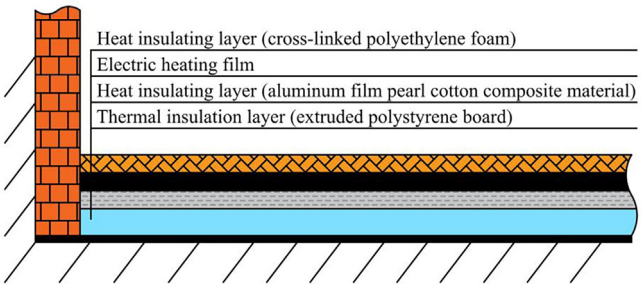


Fig. 4. Framework of radiant floor heating.

An objective experimental investigation was used to explore the thermal performance and indoor air quality of CRFH, CRFH + MV, and LTR-ISV, as shown in Fig. 5. In the thermal performance experiments, four occupants and two 100 W incandescent lamps on the ceiling were arranged as internal heat sources. Among them, occupants were simulated by hexahedron thermal manikins with the dimensions of 0.4 × 0.25 × 1.2 m (Length × Width × Height). The simulation of occupants' heat dissipation was achieved by an internal incandescent lamp (with a power of 90 W), which has been proven and widely used to simulate occupants [41,42]. As for the indoor air quality experiments, tracer gas is a suitable surrogate for evaluating indoor air quality and airborne transmission risk [43,44], of which CO_2 is widely used as it is a human respiratory product [45] and therefore was used in this study. During the experiments, four CO_2 tanks were put inside of the four thermal manikins respectively. To ensure CO_2 is released in the breathing zone of sedentary occupants, a 10 mm hole was dug 1.1 m above the surface of each thermal manikin, and a hose was used to connect the CO_2 tank to the hole in the surface of the thermal manikin. To be consistent with the amount of CO_2 exhaled by occupants, a constant flow rate was set to 320 ml/min according to Wu's study [46] and controlled by a pressure-reducing valve and a flowmeter. The experiment duration was set to 600 s to reach a steady state of CO_2 concentration with reference to the study of [47].

The subjective experiment was also conducted in the experimental room (Fig. 6) with the participation of 48 students, all of whom were non-smokers and none of whom had chronic and allergic skin diseases, and all of whom had BMI values within the healthy range. The anthropometric data are shown in Table 1. During the experiments, students were asked to wear typical winter clothing with a thermal resistance of 1.2 clo and were asked to sit in a room to read or write at an activity level of around 1.0 met. To collect students' response data, a questionnaire containing overall thermal sensation (OTS) was distributed to students. The ASHRAE 7-point scale (-3 cold, −2 cold, −1 slightly cool, 0 neutral, 1 slightly warm, 2 warm, and 3 hot) was used to assess the OTS of the occupants. After a 30-minute trial, they were asked to complete the questionnaire.



(a) Thermal experiments (b) Indoor air quality experiments

Fig. 5. Experiment conditions.



Fig. 6. Subjective experiments.

Table 1
Anthropometric data of the occupants.

Gender	Female	Male	Female + Male
Number	24	24	48
Age	20.2 ± 0.5[a]	20.3 ± 0.5	20.3 ± 0.9
Height (cm)	163.9 ± 4.6	175.9 ± 5.11	169.9 ± 9.5
Weight (kg)	52.5 ± 7.3	69.2 ± 13.3	60.9 ± 13.9
BMI (kg/m^2)	19.5 ± 2.3	22.3 ± 3.8	20.9 ± 3.8

a is the standard deviation.

During objective and subjective experiments, indoor air temperature was set to 20 °C. ISO 7730: 2005 [48] states that in areas where occupants often stay, the floor surface temperature should ideally be maintained at 19–29 °C. Hence, the floor surface temperature of CRFH and CRFH + MV was regulated to 27 °C, and could fluctuate within 26.5–27.5 °C. In the case of CRFH + MV, a dedicated outdoor air system (DOAS) was employed to supply fresh air, and the air volume depended on the density of the indoor occupants. In this case, 4.2 ACH of fresh air with an air temperature of 17 °C was served by mixing ventilation according to research [26]. In order to keep the heat supply consistent with the other two heating methods, the LTR-ISV radiant floor surface temperature and the supply air temperature were set to 24 °C and 23 °C, respectively. As for the supply ventilation rate, a related study demonstrated that the thermal performance of stratum ventilation exceeded that of mixing ventilation for the same supply ventilation rate [33]. Therefore, the LTR-ISV with a ventilation rate of 4.2 ACH did not experiment. 10 ACH was adopted according to Ref. [49], as it can provide healthy, thermal comfort and a positive pressure indoor thermal environment. In daily use, 10 ACH of supply air contains 5.8 ACH of return air and 4.2 ACH of fresh air. When indoor occupants show symptoms of virus infection, the valve at the return air duct will be switched off and the air sent into the room will be 10 ACH of fresh air. Detailed design parameters of the experiments are shown in Table 2.

2.2. System description

This section describes the components of the three heating systems for the subsequent energy and exergy analysis using MATLAB software. The component used in the systems are chosen by the water flow rate and airflow rate in the heating system. The technical parameters of components in the systems are listed in Table 3.

2.2.1. Conventional heating system

The system schematic diagram of CRFH is shown in Fig. 7**(a)**, which consists of an ASHP loop and a hot water loop. R134a is used as the working fluid in the ASHP cycle due to its efficient performance and environmental-friendly [50]. A heat exchanger is used to connect the ASHP loop and a hot water loop, allowing the transfer of heat from the heat pump to the tank. A heat exchanger is used to exchange heat between the ASHP loop and the hot water loop. The hot water is heated to 45 °C and then delivered to the room via radiant floor heating pipes.

The CRFH + MV differs from the CRFH by the installation of a DOAS, which had a built-in heat recovery module to save energy. Before being delivered indoor, the fresh air needed to go through the following four processes in the DOAS (1-3-4-5), as shown in Fig. 7**(b)**:

First pass through the primary filter,
Exchange heat with exhaust air, and heat to 17 °C by heating coil,
Then filtered through the medium efficiency filter,
Deliver the indoor by fans.

2.2.2. LTR-ISV heating system

As shown in Fig. 7**(c)**, PAU is applied in LTR-ISV. Hot water in the radiant floor pipes is heated to 40 °C before entering indoor, and then 30 °C of return water will flow through the PAU to heat the supply air. For supply air, five processes (1-2-3-4-5) need to be completed before entering indoor (1-2-3-4-5):

First pass through the primary filter,
Mix with return air,
Heated by the return water of the radiant floor pipes,
Then filtered through the medium efficiency filter,
Deliver the indoor by fans.

In addition, we used a periodic strategy to compare the energy use of CRFH + MV and LTR-ISV by dividing the day into two periods: working hours (8:30 a.m.-5:30p.m.) and non-working hours (5:30p.m.-8:30 a.m. the next day). For CRFH + MV, during non-working hours, the DOAS is turned off. For LTR-ISV, the water supply temperature is maintained at 40 °C during working hours to keep the surface temperature of the radiant floor and the supply air at 24 °C and 23 °C, respectively. During non-working hours, the PAU is turned off and the hot water tank return and supply temperatures are reduced to 35 °C and 25 °C [51], respectively.

2.3. Comparison of the heat supply

In both the CRFH and CRFH + MV modes, the radiant floor carries the indoor thermal load, while in the LTR-ISV, the radiant floor and the floor ventilation together carry the indoor thermal load. To ensure that the experiments are valid for comparison, this section compares the heat supply in the three heating modes. In CRFH, the heat supply can be calculated as follows according to the Chinese standard JGJ 142-2012 "*Technical Specification for Radiant Heating and Cooling*" [52]:

$$Q_{CRFH} = 2.13A(T_r - T_p)^{1.31} + 5 \times 10^{-8}A(T_r - T_P{}^4] \quad (1)$$

where A is the area of the radiant floor; T_r represents the temperature of the radiant floor; T_p is the area-weighted average temperature of the non-heated walls.

In CRFH + MV mode, the convective heat exchange caused by DOAS needs to be calculated according to Eq. (2). Since the fresh air temperature in CRFH + MV is lower than the indoor design air

Table 2
Experimental cases and parameters.

Case	Indoor design temperature(°C)	Surface temperature of radiant floor(°C)	Supply air temperature(°C)	Air change per hour(ACH)
CRFH	20	27 ± 0.5	–	–
CRFH + MV		27 ± 0.5	17 ± 0.5	4.2
LTR-ISV		24 ± 0.5	23 ± 0.5	10

Table 3
Technical parameter of components in the system.

Equipment	Technical data	Rated power (W)
Water pump	Nominal water flow rate: 2.0 m^3/h	90
DOAS	Nominal air flow rate: 330 m^3/h	18
PAU	Nominal air flow rate: 1000 m^3/h	249
Electric heating coil	——	400

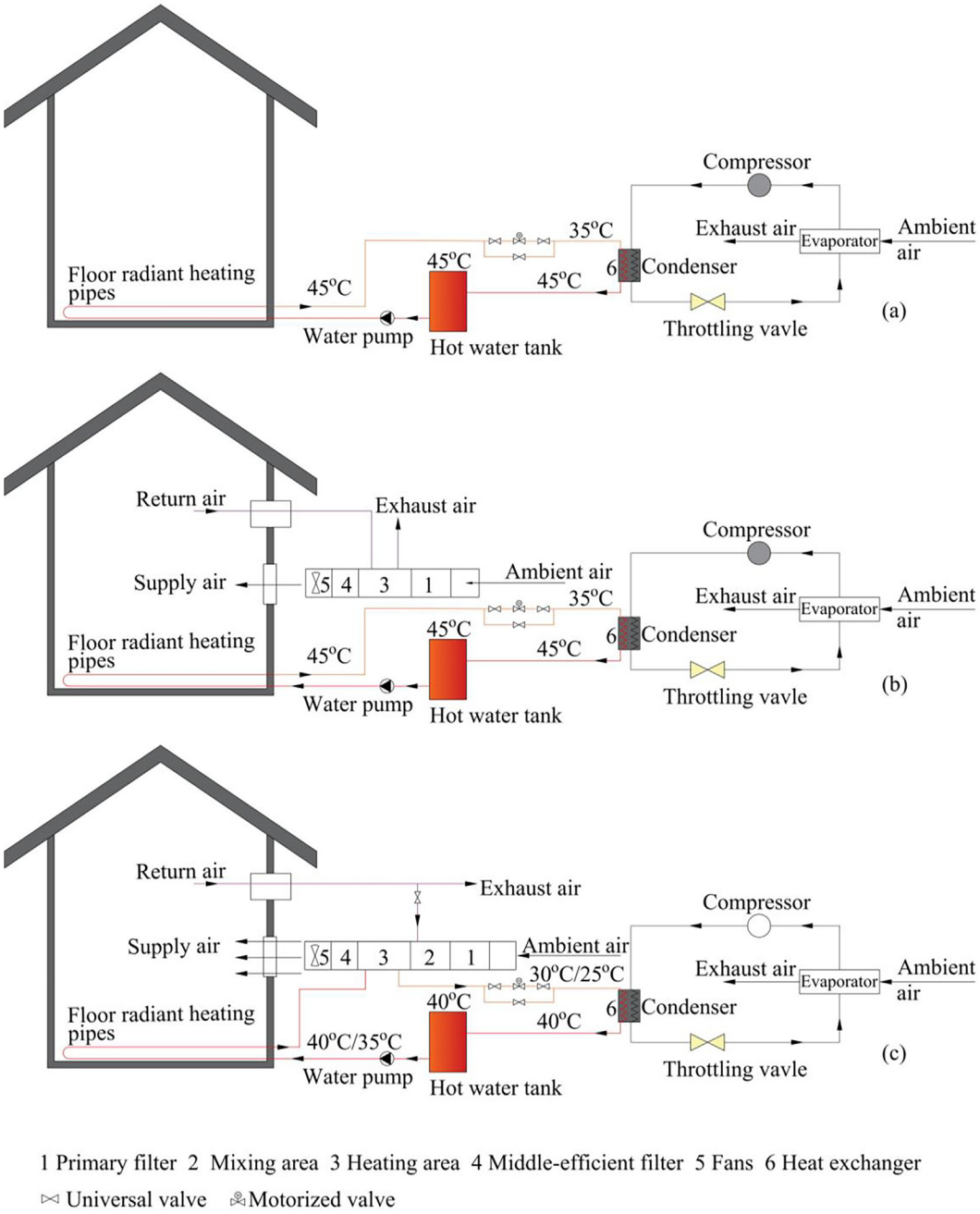


Fig. 7. (a) System schematic diagram of CRFH (b) System schematic diagram of CRFH + MV (c) System schematic diagram of LTR-ISV.

temperature, the total heat supply is the difference between radiant heat supply and convective heat supply.

$$Q_f = Gc_p(T_s - T_N) \tag{2}$$

where Q_f represents the mechanical heat load; G is the fresh air volume; c_p is the air specific heat at constant pressure, which equals to 1.01 kJ/kg·K. T_s is the supply air temperature; T_N is the indoor design air temperature.

In LTR-ISV, the total heat supply was the sum of the radiant floor heating and stratum ventilation heating. Due to the introduction of mechanical ventilation in CRFH + MV and LTR-ISV, which may result in higher convective heat transfer in the near-floor region, it is necessary to calculate and verify the convective heat transfer coefficient, which is calculated as follows:

$$Q_f = Ah_c(T_r - T_a) \tag{3}$$

$$Nu = \frac{h_c L}{k_a} \tag{4}$$

$$Nu = 0.664 Re_L^{1/2} Pr^{1/3} \; for \; \mathrm{Re}_L < 5 < 10^5 \tag{5}$$

$$\mathrm{Re}_L = \frac{\rho v L}{\mu} \tag{6}$$

where Nu is the Nusselt number; L is the Characteristic length; k_a is the thermal conductivity of air; Re_L is the Reynolds number; ρ is the density of air; μ is the dynamic viscosity of air. By calculating, the h_c in the CRFH, CRFH + MV, and LTR-ISV were within the range of 10 %.

Fig. 8 and Table 5 show the heat supply comparison of the three heating modes. Heat supply in CRFH + MV and LTR-ISV was 11.9 % lower compared with CRFH. Among them, the heat supply of radiant floor heating was 99.57 W/m^2 (CRFH and CRFH + MV) and 60.67 W/m^2 (LTR-ISV), respectively. The high heat supply is due to the poor thermal insulation of the building envelope of the experimental room. The actual heat supply of an ordinary residential building in Tianjin is approximately 50 W/m^2. Due to the high heating of the radiant floor at CRFH and CRFH + MV modes, only screeds can be laid on the floor surface in order to avoid damage to the floor material, which is not suitable for residential buildings. In practical applications, it can be achieved to use two circuits in CRFH and CRFH + MV with a water flow rate of 0.04 kg/s each by using a heating tube with a diameter of 20 mm, and one circuit with a water flow rate of 0.05 kg/s in LTR-ISV.

2.4. Measuring instruments

Thermal environment and indoor air quality parameters were measured, including air temperature, globe temperature, air velocity, and CO_2 concentration, as listed in Table 4. During thermal performance experiments, 9 vertical sampling lines (L1-L9) were evenly spaced in the experimental room to measure the air temperature distribution, as shown in Fig. 3**(a)**. Each sampling line had 11 probes with different heights (0.1 m, 0.3 m, 0.5 m, 0.7 m, 0.9 m, 1.1 m, 1.3 m, 1.5 m, 1.7 m, 1.9 m, and 2.4 m), *T*-thermocouple was used as the probe and all measuring lines were connected to data collectors for data acquisition. The position of sedentary occupants, heat flux of lamps, and cold air through windows and doors might affect the value of the globe temperature. Considering the environment has already turned into a steady-state, 1 globe thermometer was used to measure the same measurement points as the air temperature to obtain accurate values and avoid unnecessary errors. Air velocity was measured at 6 heights (0.1 m, 0.6 m, 1.1 m, 1.4 m, 1.7 m, and 2.4 m) at the same location of 9 sampling lines. According to the related study, the air exhaled by the occupants and the frequency of their breathing activity only affect thermal environment on the local area [53]. However, the measurement points in this research were all located more than 20 cm away from the occupants' breathing zone, which is focused on obtaining the whole thermal environment. Hence, the effect caused by the human breathing activity can be negligible. For the CO_2 concentration in the breathing zone, a respiratory zone radius of 10 cm with reference to Lidén's study was employed [53]. The sensors were placed 100 mm in front of each thermal manikin CO_2 release hole (1.1 m). And another sensor was put near the outlet to monitor the outlet CO_2 concentration. In addition, the outdoor and supply CO_2 concentrations were monitored before the experiment. The corresponding data was collected by the Hobo data logger. Since the variables are directly measured and require measurement of instrumental uncertainty. The measurement uncertainties related to the repetition of the experiments (σ) and sensor accuracy were calculated (see Table 4 for details). For uncertainties related to the repetition of the experiments, which is calculated as:

$$\sigma = \left[\sum (x_i - x)^2 / (n-1)\right]^{1/2} \tag{7}$$

where x_i is the data value of each measurement; x is the average value of n measurements. After calculation, the air temperature, air speed, and CO_2 measurement accuracy of this experiment are 0.2 %, 0.88 % and 0.95 %, respectively.

2.5. Indoor thermal comfort and energy performance criteria

In order to evaluate and compare the performance of CRFH, CRFH + MV, and LTR-ISV, the following criteria are analyzed:

(1) Operative temperature,
(2) Air velocity distribution and draft sensation,
(3) Overall Thermal Sensation,
(4) Zone air distribution effectiveness (CO_2 removal efficiency),
(5) Local relative contaminant exposure index,

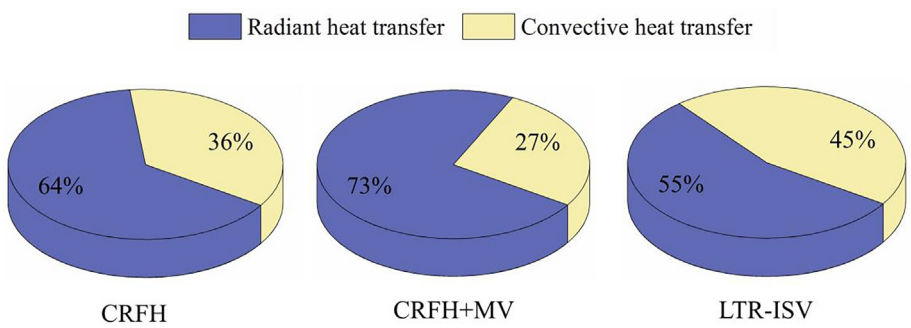


Fig. 8. Comparison of the heat supply composition ratio.

Table 4
Detailed information on measuring instruments.

Physical parameter	Instrument	Range	Accuracy
Indoor air temperature	*T*-thermocouple	−200–260 °C	±0.06 °C (15–25 °C)
Globe temperature	AZ8778	0–80 °C	±1 °C
Indoor air velocity	Testo 440	0–5 m/s	±0.03 m/s or ±4 % of the measuring data
CO_2 concentration	Telaire 7001	0–10000 ppm	±50 ppm

Table 5
Specific values of heat supply composition.

Heating mode	CRFH	CRFH + MV	LTR-ISV
Radiant heat supply (W)	2273.6	2273.6	1707.1
Convective heat supply (W)	1263.8	844.8	1409.2
Radiant floor heat supply (W)	3537	3537	2115
Mechanical ventilation heat supply (W)	–	−419	961
Total (W)	3537	3118	3116

(6) Airborne transmission risk assessed by the modified Wells-Riley equation.

Operative temperature, which is influenced by convection and radiation simultaneously, is appropriate to analyze these three heating modes. It can be calculated as follows:

$$T_o = \frac{h_r \bar{T}_r + h_c T_a}{h_r + h_c} \tag{8}$$

where T_o is the operative temperature; $\bar{T}_r$ is the indoor mean radiant temperature; t_a represents the indoor air temperature; h_r is the radiative heat-transfer coefficient; h_c is the convective heat-transfer coefficient. When v_a < 0.2 m/s, h_r and h_c are considered equal; when 0.2 m/s < v_a < 0.6 m/s, the values of h_r and h_c are considered to be in the ratio of 4:6 [54].

Air velocity was measured during the experiment to evaluate draft sensation due to the higher air velocity caused by mechanical ventilation. Since the occupants in the experiment were assumed to be sedentary, the draft rate (*DR*) index was used according to ISO 7730, and can be expressed as Eq. (9):

$$DR = (34 - T_a)(v_a - 0.05)^{0.62}(0.37\, v_a Tu + 3.14) \tag{9}$$

If v_a < 0.05 m/s, calculated as v_a = 0.05, if *DR* greater than 100 %, calculated as *DR* = 100 %. *Tu* is the turbulence intensity, which is calculated as follows:

$$Tu = \frac{v_{sd}}{\bar{v}} \times 100\% \tag{10}$$

where v_{sd} is the standard deviation of air velocity; $\bar{v}$ is the average velocity. Turbulence intensity increases as the velocity decreases or velocity fluctuation increases.

Zone air distribution effectiveness, also known as contaminant removal efficiency, is a relative value used to evaluate indoor air quality. It shall be calculated by Eq. (11):

$$E_Z = \frac{c_e - c_s}{c - c_s} \tag{11}$$

where c is the average contaminant concentration in the breathing zone; c_e is the average contaminant concentration of the outlets; c_s is the average contaminant concentration of the air inlets. The above values are direct measurements as the effect of background CO2 has been excluded from the equation [55]. Air quality is better with higher E_Z values.

The exposure to contaminants of healthy occupants can be calculated by local relative contaminant exposure index, which has been widely used as an important index in airborne transmission studies [56,57], and is defined as the reciprocal of contaminant removal efficiency:

$$e_p^c = \frac{c_i - c_s}{c_e - c_s} \tag{12}$$

where c_i is the concentration of the tracer gas for a certain point.

The Wells-Riley equation is a popular and classic method for predicting airborne transmission risk, and the original equation is in the following form:

$$P_I = 1 - \exp(\frac{\mathrm{Iqpt}}{V}) \tag{13}$$

where P_I is the predicted airborne transmission risk; *I* is the infected individuals, in this case, *I* = 1. *p* is the pulmonary ventilation rate, when occupants stay sedentary or doing light activities, *p* = 0.3 m^3/h. *q* is the quantum generation rate, *q* differs with the virus species and the vulnerability of the people, for the COVID-19 virus, *q* = 0.238 quantum/s [58]. *t* is the exposure time; *V* is the ventilation rate of the experimental room.

The original formula had a limitation in that it assumed that indoor air was completely mixed and was only affected by exposure time and ventilation rate. To solve this deficiency, related researchers have made different modifications to make the formula more suitable for their research [59]. In this study, stratum ventilation, which belongs to non-uniform ventilation was applied in the experiment, in order to make the Wells-Riley equation suitable for non-uniform ventilation modes, E_Z was thus introduced in the equation according to [58], as shown in the following:

$$P_I = 1 - \exp(\frac{\mathrm{Iqpt}}{V \cdot E_Z}) \tag{14}$$

2.6. Energy and exergy efficiency analysis

We used MATLAB software to calculate the coefficient of performance (COP). To simplify the process of the system, some assumptions needed to be undertaken before simulation [60]:

(1) All the system cycles and components are in a steady-flow state,

(2) The friction loss, pressure drop, as well as heat loss of the refrigerant and hot water in components and pipes are all ignored,

(3) The influence of potential and kinetic energy changes in working fluids and hot water are neglected,

(4) The throttling and compression progress are considered isenthalpic.

COP is defined as the ratio of heat supply and power consumption of the whole system:

$$COP = \frac{Q}{W} = \frac{Q}{W_{comp} + W_{wp} + W_{me}} \tag{15}$$

where *Q* is the output heat, which is the heat supply calculated in Section 2.3; *W* is the input power;W_{comp} is the power consumption of the compressor in the ASHP; W_{wp} is the input power of water pump in the hot water loop; W_{me} is the input power in mechanical ventilation.

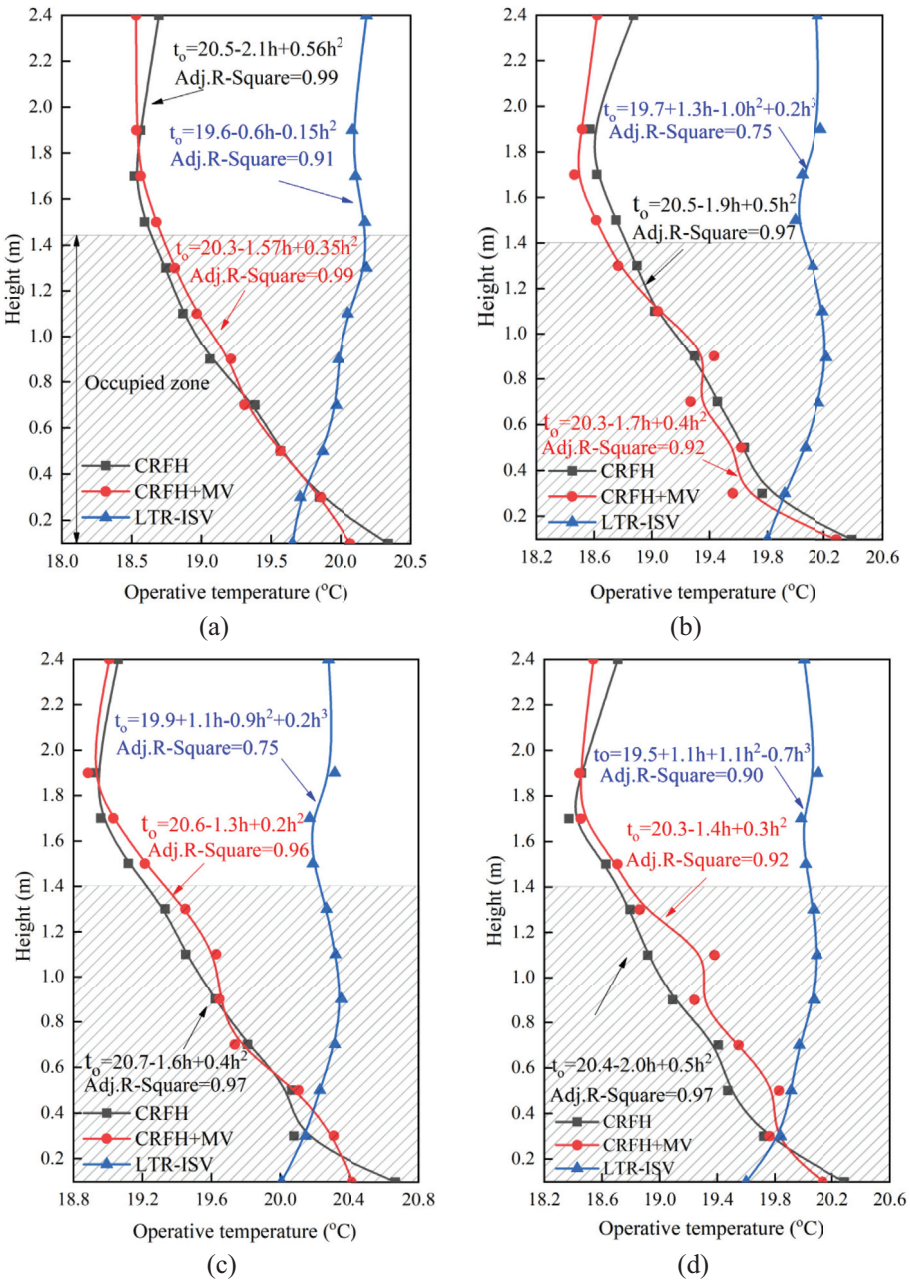


Fig. 9. (a)Vertical distribution of overall averaged operative temperature, (b) Comparison of vertical temperature distribution in L2, (c) Comparison of vertical temperature distribution in L5, and (d) Comparison of vertical temperature distribution in L8.

Since there is no mechanical ventilation, the COP in CRFH is calculated in the following:

$$COP = \frac{Q_{CRFH}}{W_{comp} + W_{wp}} \tag{16}$$

where Q_{CRFH} is the heat supply of CRFH.

In CRFH + MV, the fan and heating coil in the DOAS is added to the input power:

$$COP = \frac{Q_{CRFH+MV}}{W_{comp} + W_{fan} + W_{hc} + W_{wp}} \tag{17}$$

where $Q_{CRFH+MV}$ is the heat supply of CRFH + MV; W_{fan} is the rated power of the fans; W_{hc} is the rated power of the heating coil in the DOAS.

As for LTR-ISV, owing to that the energy used for heating fresh air is provided by ASHP, the power use of PAU only contains fans:

$$COP = \frac{Q_{LTR-ISV}}{W_{comp} + W_{fan} + W_{wp}} \tag{18}$$

where $Q_{LTR-ISV}$ is the heat supply of LTR-ISV.

Exergy (ex) is defined as the maximum useful work produced by the system with the process that working fluid from initial statement (p, T) reversible transition to the ambient statement (p_0, T_0), it can be expressed as follows:

$$ex = h_i - h_0 - T_0(s_i - s_0) \tag{19}$$

where h is the enthalpy; s is the entropy; subscript 0 stands for the dead state of the environment.

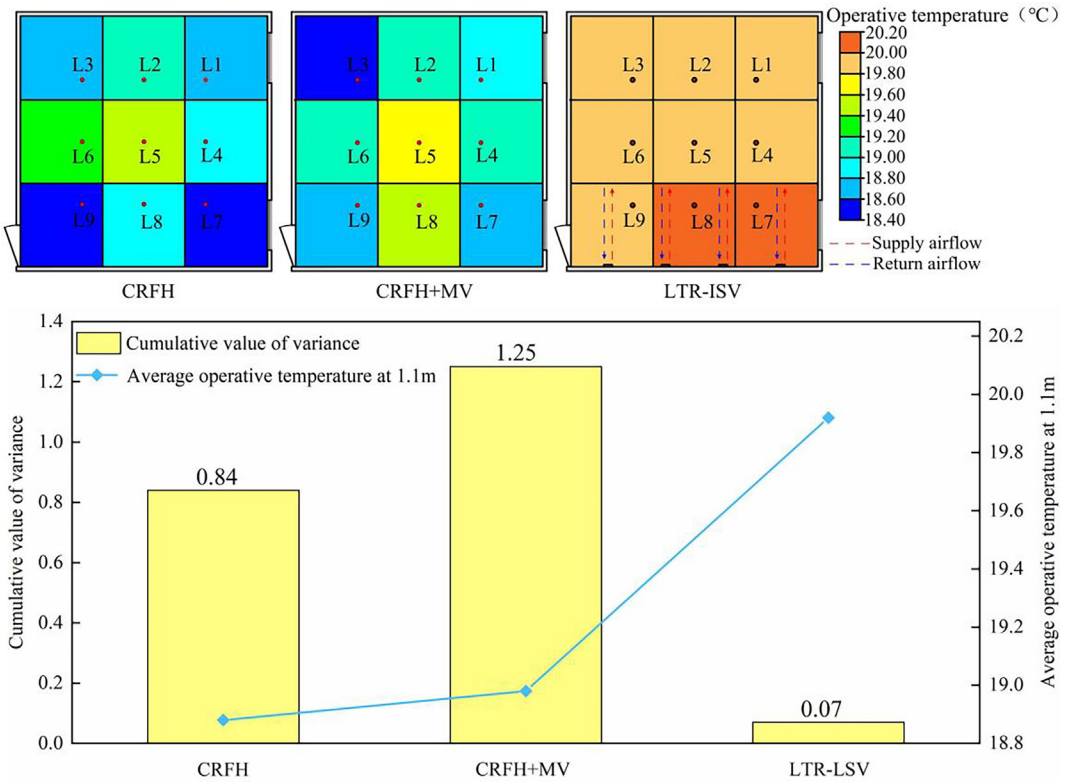


Fig. 10. Horizontal distribution of operative temperature at 1.1 m plane.

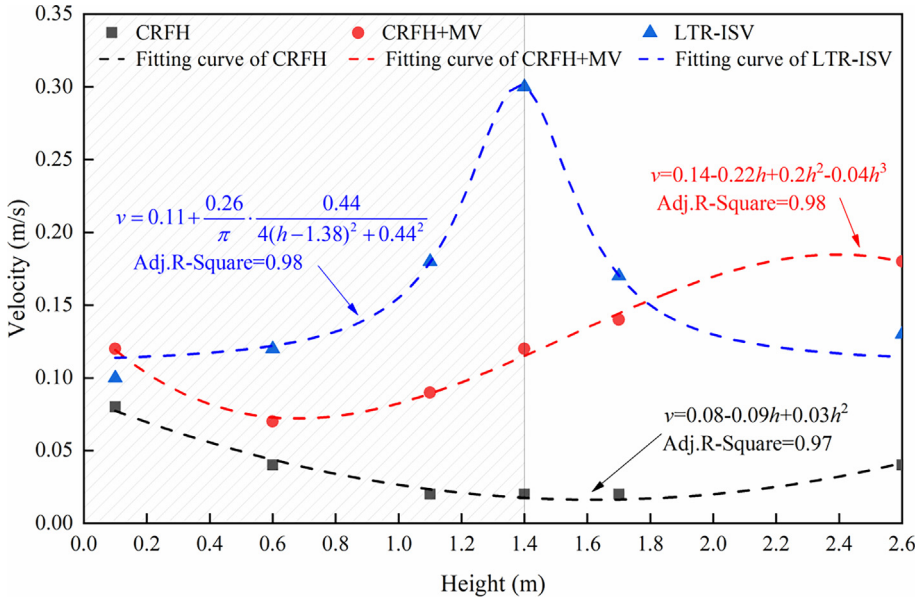


Fig. 11. Comparison of the vertical average velocity distribution.

The energy analysis in this study is based on hot water and moist air (working fluids). The exergy calculation of hot water can be directly calculated according to Eq. (19). As for moist air, mechanical ventilation exists in the system of CRFH + MV and LTR-ISV to deal with moist air, the exergy of a unit mass of moist air is composed of thermal exergy (ex_{th}), chemical exergy (ex_{ch}), and mechanical exergy (ex_{me}) and influenced by pressure (P), temperature (T), partial pressure of water vapor (P_v) and dry air (P_a). As shown in Eq. ((20)–(23)) [40].

$$ex_{th} = (C_{p,da} + wC_{p,v})(T - T_0) - T_0(C_{p,da} + wC_{p,v})\ln\frac{T}{T_0} \tag{20}$$

$$ex_{ch} = T_0 R_{da}\ln\frac{x_{da}}{x_{da,0}} + wT_0 R_v \ln\frac{x_v}{x_{v,0}} \tag{21}$$

$$ex_{me} = T_0(R_{da} + wR_v)\ln\frac{P}{P_0} \tag{22}$$

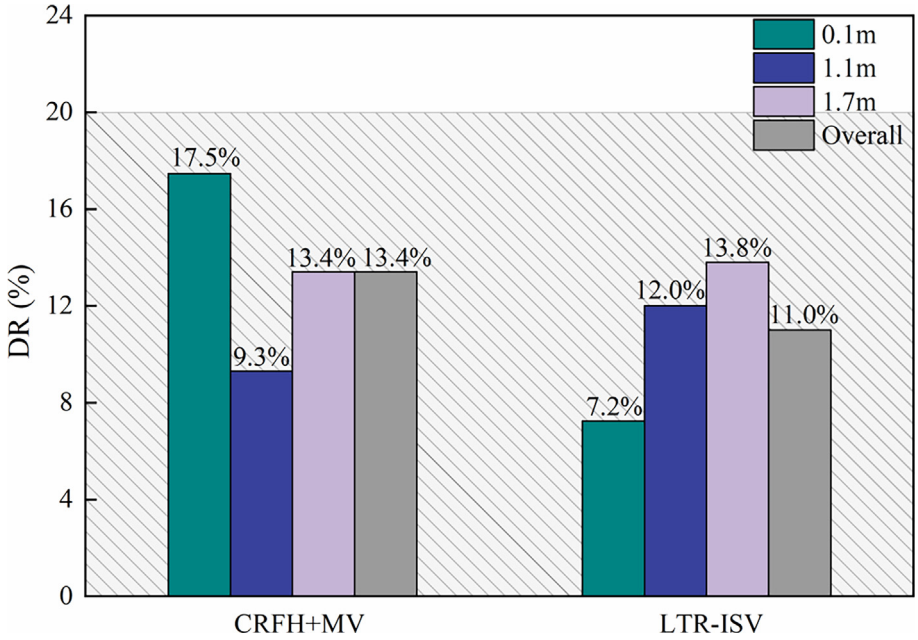


Fig. 12. Comparison of the local and overall *DR*.

$$ex_a = ex_{th} + ex_{ch} + ex_{me} \tag{23}$$

where $C_{p.da}$ is the moist air specific heat; w is the humidity ratio; $C_{p,v}$ is the water vapor specific heat; R_{da} is the dry air ideal gas constant. Since P and P_0 are basically equal, ex_{me} can be ignored, so the calculation can be simplified as follows:

$$\begin{aligned} ex = &\left[C_{p,da}(T - T_0) - T_0\left(C_{p,da}\ln\frac{T}{T_0} - R_{da}\ln\frac{p_{da}}{p_{da,0}}\right)\right] \\ &+w\left[C_{p,v}(T - T_0) - T_0 - T_0\left(C_{p,v}\ln\frac{T}{T_0} - R_v\ln\frac{p_v}{p_{v,0}}\right)\right] \end{aligned} \tag{24}$$

The exergy efficiency of the whole system is employed, which is defined as the ratio of total exergy input and total exergy output:

$$\eta = \frac{ex_{out}}{ex_{in}} \tag{25}$$

where η is the exergy efficiency; ex_{out} is the output exergy. The system is more ideal with η increases.

3. Results and discussion

3.1. Operative temperature

The operative temperature distribution of the three heating modes is shown in Fig. 9**(a)**. The average operative temperature of LTR-ISV was more uniform compared to the other two heating modes, which was attributed to the introduction of the large air volume, as it enhances indoor air mixing. Besides, under the premise of the same heat supply, the average operative temperature of LTR-ISV reached 19.89 °C, while the corresponding values for CRFH and CRFH + MV were 19.11 °C and 19.01 °C, respectively. LTR-ISV was 0.88 °C and 0.98 °C higher than CRFH and CRFH + MV.

To compare the operative temperature parallel to the direction of supply air, a vertical plane through the center, which contained three measuring points of L2, L5, and L8 was used, as shown in Fig. 9**(b), (c), (d)**. The result showed that in the occupied zone (0.1–1.4 m), the operative temperature of LTR-ISV was the highest with a value of 20.08 °C, while that of CRFH and CRFH + MV was 19.58 °C and 19.23 °C respectively. It indicated that the average temperature for the occupied zone served by LTR-ISV was 0.50 °C and 0.85 °C higher than CRFH and CRFH + MV.

In the aim to explore the uniformity of the operative temperature on the horizon plane, the distribution of operative temperature at 1.1 m is compared in Fig. 10. It shows the operative temperature of CRFH and CRFH + MV were peaked at L5, other measuring points, which were near cold walls, door, or windows, were influenced by the cold radiation and showed a lower operative temperature. The maximum operative temperature difference of CRFH and CRFH + MV was 0.9 °C and 1.2 °C, respectively. This indicated that the application of CRFH + MV worsen the radiant asymmetry of CRFH, but the corresponding value for LTR-ISV was only 0.38 °C, and the cumulative value of the operative temperature variance at different measuring points was only 0.07, indicating the heat supply was fully utilized and evenly distributed throughout the room.

3.2. Air velocity

Fig. 11 shows the vertical distribution of the mean air velocity. In the occupied zone, the mean velocities of 0.04 m/s, 0.1 m/s, and 0.18 m/s for CRFH, CRFH + MV, and LTR-ISV, respectively, are within the thermal comfort range. CRFH had the lowest velocity and a large vertical temperature difference, and that was because the only driving force was the density difference between the warm floor and room air temperature. For the other two heating modes that contained mechanical ventilation, indoor mixing was enhanced and vertical differences in average velocity were small. The CRFH velocity shows higher values in the areas near the floor and ceiling, which is the result of the strong convection effect occurring from the large temperature difference between the air and the walls. The same phenomenon was observed in the floor area of CRFH + MV, the air velocity was increased as the heights raises due to the ceiling-mounted inlets. For LTR-ISV, the velocity peak appeared at the height of 1.4 m, which was due to the combined effect of the location of the supply air inlet and buoyancy force.

Since air velocity in LTR-ISV at 1.4 m reached 0.3 m/s, it is necessary to evaluate whether the higher velocity would lead to uncomfortable draught or not. *DR* was calculated by using Eq. (9)-(10), and the acceptable range is between 0 and 20 % [61].

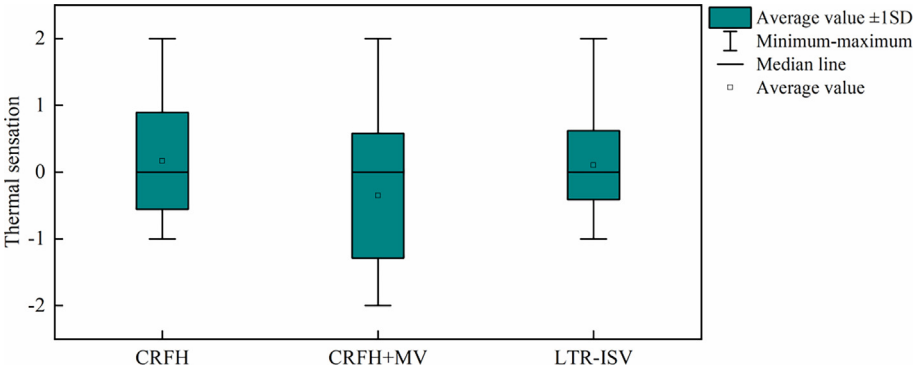


Fig. 13. OTS of students.

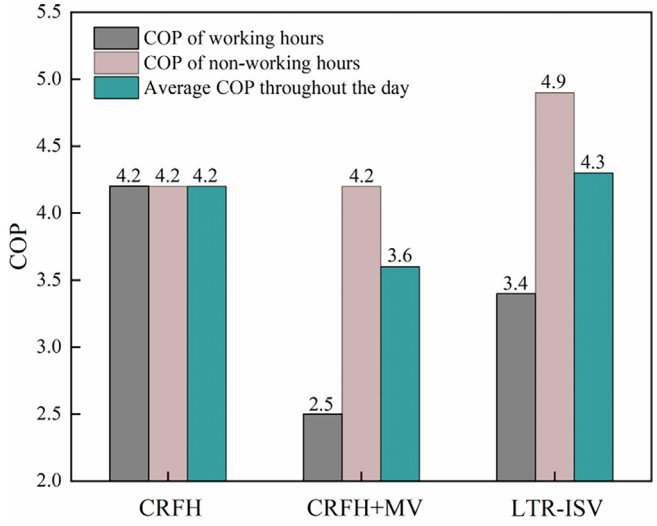


Fig. 14. COP of three systems with the different period.

Table 6
Performance of the three systems.

CRFH system	ex_{in}(kW)	ex_{out}(kW)	ex_{loss}(kW)	η(%)
Heat pump	38.18	28.99	9.19	75.93
Radiant floor heating	28.99	22.35	6.64	77.10
Total	67.17	51.34	15.38	76.43
CRFH + MV system	ex_{in}(kW)	ex_{out}(kW)	ex_{loss}(kW)	η(%)
Heat pump	38.18	28.99	9.19	75.93
Radiant floor heating	28.99	22.35	6.64	77.10
DOAS	26.59	9.33	17.66	35.09
Total	93.76	60.67	33.49	64.71
LTR-ISV system	ex_{in}(kW)	ex_{out}(kW)	ex_{loss}(kW)	η(%)
Heat pump	34.5	27.03	7.47	78.35
Radiant floor heating	27.03	24.05	2.98	88.98
PAU	24.29	19.02	5.27	78.30
Total	85.73	70.10	15.72	81.77

The *DR* of CRFH and LTR-ISV, including ankle level (0.1 m), breathing zone level (1.1 m), and standing level (1.7 m) is shown in Fig. 12. As the velocity was generally<0.05 m/s, the DR value was equal to 0 in CRFH. It can be seen that both LTR-ISV and CRFH + MV had acceptable *DR* values below 20 %, and the overall *DR* value was 13.4 % and 11.0 % for CRFH + MV and LTR-ISV, respectively. The noticeable difference was found at ankle level, with a higher velocity and turbulence intensity, the local *DR* at 0.1 m was higher in CRFH + MV. Therefore, LTR-ISV can notably enhance indoor air mixing without causing an additional draft sensation.

3.3. Ots

The OTS of the students under three heating modes is shown in Fig. 13. According to ISO 7730, which stated that the OTS was better within the range of −0.5–0.5. The average OTS of CRFH, CRFH + MV, and LTR-ISV was 0.2, −0.4, and 0.1 respectively, indicating the three heating modes all had rather thermal comfort environments. The relatively low OTS value in CRFH + MV was the introduction of fresh cold air, where the cold air was deposited to near floor region and thus a rather low local air temperature. Besides, the OTS in LTR-ISV was more concentrated, which indicated the indoor air temperature was relatively uniform.

3.4. Energy-saving efficiency and exergy analysis

The energy performance (COP) in the working hours and non-working hours and the exergy performances during the working hours were calculated and shown in Fig. 14 and Table 6. During the working hours, the COP for CRFH, CRFH + MV, and LTR-ISV was 4.2, 2.5, and 3.4, respectively. The difference in COP during this period is due to the addition of mechanical ventilation in CRFH + MV and LTR-ISV. CRFH + MV has the smallest COP because the heating coils in DOAS are driven by electricity, which can only reach a COP value of 1. During the non-working hours, the difference in COP in this period is due to the supply water temperature in radiant floor heating. With the mechanical ventilation turned off and the supply water temperature decreased to 35 °C, the COP value of LTR-ISV reached a COP value of 4.9 which is 0.6 and 1.3 higher than CRFH and CRFH + MV, respectively, indicating that the regulation strategy is effective.

In exergy analysis, LTR-ISV showed the highest exergy efficiency with a value of 81.77 %, while that of CRFH and CRFH + MV were 76.43 % and 64.71 %, respectively. Indicating the hot water loop noticeably enhanced the exergy performance. While the heating coils accounted for 60 % of the total energy loss in the CRFH + MV system. It is noted that the 40 °C water supply temperature reduced the initial input energy provided by the heat pump of the LTR-ISV, which emphasizes the low-grade energy use of the LTR-ISV.

Electricity consumption is also an important parameter for revealing energy performance. In this study, electricity consumption is calculated for the whole day and the whole operating season. In cold regions of China, the entire heating season starts on November 15th and ends on March 15th the next year (120 days). The results are shown in Table 7. With the addition of DOAS, the electricity of CRFH + MV increased by 103.7 % compared with

Table 7
Electric usage of three heating systems.

Heating system	One day (kWh)	Whole operating season (kWh)
CRFH	22.4	2684.2
CRFH + MV	45.6	5468.4
LTR-ISV	38.4	4614.2

CRFH. The electricity consumption of LTR-ISV was 4614.2 kWh. Due to the introduction of fresh air, electricity consumption for LTR-ISV system was higher than that of CRFH, and had a limited effect on reducing electricity consumption compared to CRFH + MV. On the one hand, it indicated that the LTR-ISV heating system can reduce energy consumption with better thermal comfort and indoor air quality compared to CRFH + MV, but on the other hand, it also indicated that the heat load distribution between radiant floor and floor ventilation needs to be further optimized.

3.5. Indoor air quality

3.5.1. CO_2 removal efficiency

In order to assess the performance of three heating systems in pollutant removal, CO_2 removal experiments were conducted, and the results are shown in Fig. 15. Due to the absence of mechanical ventilation in CRFH, the CO_2 concentration was continuously rising during the first 300 s and reached 2712 ppm. If people stay indoors for a long period, they inevitably had to open the windows to obtain fresh air. CRFH + MV had a limited effect on reducing the CO_2 concentration, which was stable at 1742 ppm at 200 s. Due to a ventilation flow rate that was 2.7 times higher than that of CRFH + MV, the CO_2 concentrations for the first and second row occupants in the LTR-ISV were 1259 ppm and 1448 ppm, respectively, both lower than those in the CRFH and CRFH + MV. The reason for the higher concentration in the second row was due to two reasons: 1) the air velocity in the second row is smaller due to the velocity decay along the air inlet and the blockage of occupants in the first row, and 2) The supply air arriving at the second row is contaminated with CO_2 generated by the occupants in the first row. Table 8 shows the contaminant removal efficiency of these three heating modes, the E_Z value of LTR-ISV was 1.15 higher than CRFH + MV. This indicates that LTR-ISV can remove indoor pollutants faster and with higher contaminant removal efficiency.

Table 8
Contaminant removal efficiency of the experimental cases.

Index	CRFH	CRFH + MV	LTR-ISV
E_Z	–	0.93	2.08

Table 9
Relative contaminant exposure index.

Index	CRFH	CRFH + MV	LTR-ISV	
			Row 1	Row 2
e_p^c	–	1.08	0.44	0.52

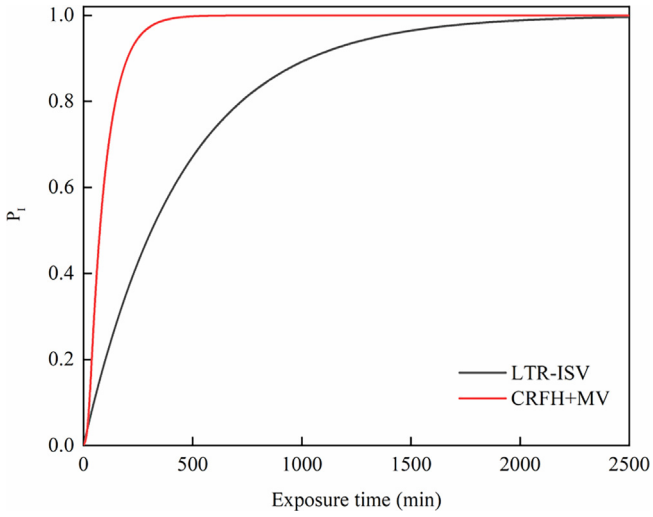


Fig. 16. Predicted probability of airborne transmission risk for CRFH + MV and LTR-ISV.

3.5.2. Airborne transmission risk evaluation

e_p^c and P_I are discussed in this section. e_p^c is applied to show the exposure to contaminants near the breathing point. The results are shown in Table 9. The testing point arrangement was the same as the CO_2 concentration experiment. The value of CRFH + MV was much higher than LTR-ISV, indicating a higher contaminant exposure rate was presented in all probes of CRFH + MV. In LTR-ISV, as

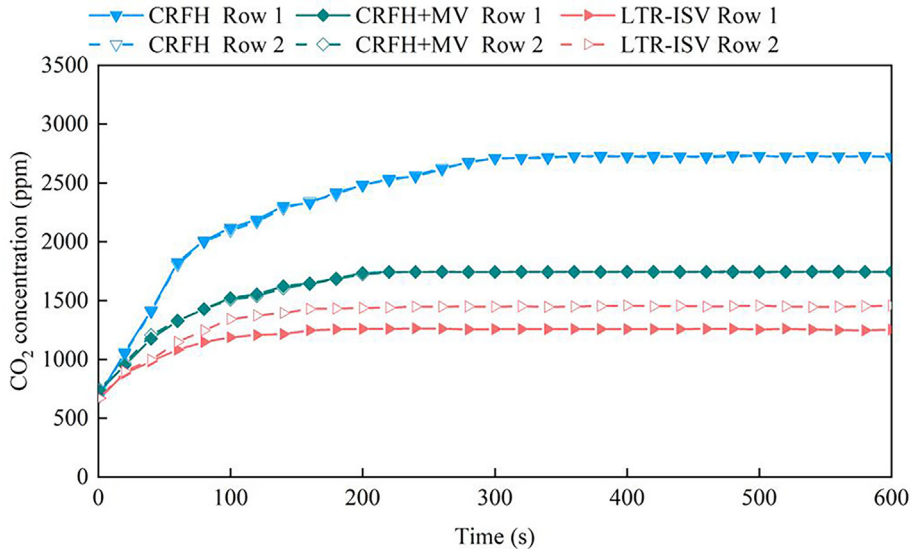


Fig. 15. Trend of CO_2 concentration in the experiment.

the distance between the air inlets and positions of occupants were different, the first row of occupants was 0.08 less exposed with a e_p^c value of 0.44, and the difference was acceptable. The value of the first row and second row in LTR-ISV was 0.64 and 0.56 lower than that of CRFH + MV, indicating LTR-ISV can serve a low-exposed indoor environment.

Assuming that only 1 infector stayed indoor, the probability of the predicted airborne transmission risk was calculated and shown in Fig. 16. The exposure time was defined long enough for the probability values approach to 1 (100 %), and the results illustrated that the risk of airborne transmission for CRFH + MV took 6.7 h to reach 1, while LTR-ISV took 36.3 h, indicating CRFH + MV was 5.45 times faster than that of LTR-ISV. The P_I values are expected to be low for safety concerns. Take 10 % for example, the time before the P_I value reached 10 % only took 98 s in CRFH + MV, while the corresponding time for LTR-ISV was 668 s. The results also showed that the airborne transmission risk in LTR-ISV tended to increase more slowly and had a significantly lower risk of airborne transmission than CRFH + MV for the same exposure time.

4. Conclusions

With aim of enhancing indoor air quality and saving energy, the LTR-ISV system was proposed, and experimental investigations were applied to study thermal performance, airborne transmission risk control, and indoor pollutant removal. Building energy efficiency was simulated by MATLAB and exergy analysis was also calculated.

(1) For the thermal environment, the operative temperature of LTR-ISV was 0.78 °C and 0.88 °C higher than CRFH and CRFH + MV, and little temperature fluctuation occurred on the vertical plane. The velocity field of LTR-ISV was distributed as a "sandwich" in the vertical plane, the highest air velocity was 0.3 m/s at 1.4 m due to the ventilation flow rate being 2.38 times higher, and no additional draught occurred.

(2) The average COP of LTR-ISV, CRFH, and CRFH + MV was 4.2, 2.9, and 4.3, respectively. The exergy efficiency of LTR-ISV, CRFH, and CRFH + MV was 81.77 %, 76.43 %, and 64.71 % respectively, indicating the higher exergy efficiency of LTR-ISV. The electricity usage (CRY) for the whole operating season was 1342.1, 2734.2, and 2307.1, respectively. The higher electricity usage of LTR-ISV is primarily due to the PAU.

(3) LTR-ISV can remove indoor contaminants and dilute virus concentration more effectively. The CO_2 concentration value of LTR-ISV was 400 ppm less than CRFH + MV on average. The relative exposure rate of the first row and second row of occupants are only 0.44 and 0.52. The airborne transmission risk was 5.35 times lower under the same exposure time.

The findings of this study reveal the potential application prospects of the LTR-ISV system and provide a new direction for the space heating system. However, this study still has certain limitations. The high heat supply in the experimental room, which was caused by the poor thermal insulation of the building envelope, increased the heating demand to a high level (usually approximately 50 W/m^2). In the evaluation of airborne transmission risk, the impacts of social distance and wearing masks were ignored. And only one heat supply ratio between the stratum ventilation and radiant floor heating was studied in LTR-ISV. In further investigations, the potential of LTR-ISV used in residential buildings, especially in remote areas, will be investigated in response to the Chinese government's aggressive "clean heating" program. The heating ratio of radiant floor heating and stratum ventilation in LTR-ISV will also be further optimized. In addition, intelligent and flexible measures can be used to improve the performance of LTR-ISV, such as developing a smartphone app that helps users to control the on and off state or adjust relevant parameters of low-temperature radiant floor and stratum ventilation.

Data availability

Data will be made available on request.

Declaration of Competing Interest

The authors declare that they have no known competing financial interests or personal relationships that could have appeared to influence the work reported in this paper.

Acknowledgment

This work is supported by National Natural Science Foundation of China (Project No. 52008147), and Hebei Province Funding Project for Returned Scholars, China (Project No. C20190507).

References

[1] BERC, International Energy Agency (IEA) District Energy Systems in China: Options for Optimisation and Diversification, 2017.
[2] T. University, Annual Development Research Report on Building Energy Efficiency in China 2020, China Construction Industry Press, 2020.
[3] G. Feng, G. Wang, Q. Li, Y. Zhang, H. Li, Investigation of a solar heating system assisted by coupling with electromagnetic heating unit and phase change energy storage tank: towards sustainable rural buildings in northern China, Sustain. Cities Soc. 80 (2022).
[4] S. Zhang, X. Wang, Y. Li, W. Wang, W. Li, Study on a novel district heating system combining clean coal-fired cogeneration with gas peak shaving, Energy Convers. Manage. 203 (2020).
[5] M. Deng, R. Ma, F. Lu, Y. Nie, P. Li, X. Ding, Y. Yuan, M. Shan, X. Yang, Techno-economic performances of clean heating solutions to replace raw coal for heating in Northern rural China, Energy Build. 240 (2021).
[6] Y. Zhang, Q. Ma, B. Li, X. Fan, Z. Fu, Application of an air source heat pump (ASHP) for heating in Harbin, the coldest provincial capital of China, Energy Build. 138 (2017) 96–103.
[7] M. Deng, Y. Nie, F. Lu, R. Ma, Y. Yuan, M. Shan, X. Yang, Pollutant emission performances of improved solid fuel heating stoves and future implications in rural China, Energy Build. 257 (2022).
[8] S. Liang, T. Zhang, Y. Wang, X. Jia, Sustainable urban materials management for air pollutants mitigation based on urban physical input–output model, Energy 42 (1) (2012) 387–392.
[9] Z. Liu, S. Ma, G. Cao, C. Meng, B.-J. He, Distribution characteristics, growth, reproduction and transmission modes and control strategies for microbial contamination in HVAC systems: a literature review, Energy Build. 177 (2018) 77–95.
[10] WHO, WHO Coronavirus (COVID-19) Dashboard, 2022. https://covid19.who.int/. (Accessed 11 July 2022.
[11] CDC, Social distancing, quarantine, and isolation. Centers for Disease Control and Prevention, 2020.
[12] M. Jayaweera, H. Perera, B. Gunawardana, J. Manatunge, Transmission of COVID-19 virus by droplets and aerosols: a critical review on the unresolved dichotomy, Environ. Res. 188 (2020).
[13] J.J. Quiñones, A. Doosttalab, S. Sokolowski, R.M. Voyles, V. Castaño, L.T. Zhang, L. Castillo, Prediction of respiratory droplets evolution for safer academic facilities planning amid COVID-19 and future pandemics: a numerical approach, J. Build. Eng. (2022).
[14] M. Qian, J. Jiang, COVID-19 and social distancing, J. Public Health (2020) 1–3.
[15] A.M. Aliyu, D. Singh, C. Uzoka, R. Mishra, Dispersion of virus-laden droplets in ventilated rooms: effect of homemade facemasks, J. Build. Eng. 44 (2021).
[16] W. Liu, L. Liu, C. Xu, L. Fu, Y. Wang, P.V. Nielsen, C. Zhang, Exploring the potentials of personalized ventilation in mitigating airborne infection risk for two closely ranged occupants with different risk assessment models, Energy Build. 253 (2021).
[17] J. Wang, J. Huang, Q. Fu, E. Gao, J. Chen, Metabolism-based ventilation monitoring and control method for COVID-19 risk mitigation in gymnasiums and alike places, Sustain. Cities Soc. 80 (2022).
[18] H. Motamedi, M. Shirzadi, Y. Tominaga, P.A. Mirzaei, CFD modeling of airborne pathogen transmission of COVID-19 in confined spaces under different ventilation strategies, Sustain. Cities Soc. 76 (2022).
[19] X. Kong, C. Guo, Z. Lin, S. Duan, J. He, Y. Ren, J. Ren, Experimental study on the control effect of different ventilation systems on fine particles in a simulated hospital ward, Sustain. Cities Soc. 73 (2021).
[20] B. Blocken, T. Van Druenen, T. Van Hooff, P. Verstappen, T. Marchal, L.C. Marr, Can indoor sports centers be allowed to re-open during the COVID-19 pandemic based on a certificate of equivalence?, Build Environ. 180 (2020).

[21] X. Wu, J. Zhao, B.W. Olesen, L. Fang, F. Wang, A new simplified model to calculate surface temperature and heat transfer of radiant floor heating and cooling systems, Energy Build. 105 (2015) 285–293.
[22] Q. Li, J. Wu, H. Liu, T. Pan, Y. Li, Experimental research on office building solar capillary heating system, Procedia Eng. 121 (2015) 2021–2028.
[23] A. Zarrella, M. De Carli, C. Peretti, Radiant floor cooling coupled with dehumidification systems in residential buildings: a simulation-based analysis, Energy Convers. Manage. 85 (2014) 254–263.
[24] L. Kempton, D. Daly, G. Kokogiannakis, M. Dewsbury, A rapid review of the impact of increasing airtightness on indoor air quality, J. Build. Eng. 57 (2022).
[25] P. Brinks, O. Kornadt, R. Oly, Development of concepts for cost-optimal nearly zero-energy buildings for the industrial steel building sector, Appl. Energy 173 (2016) 343–354.
[26] X. Wu, B.W. Olesen, L. Fang, J. Zhao, A nodal model to predict vertical temperature distribution in a room with floor heating and displacement ventilation, Build. Environ. 59 (2013) 626–634.
[27] S. Liu, M. Koupriyanov, D. Paskaruk, G. Fediuk, Q. Chen, Investigation of airborne particle exposure in an office with mixing and displacement ventilation, Sustain. Cities Soc. (2022) 103718.
[28] X. Wu, L. Fang, B.W. Olesen, J. Zhao, Air distribution and ventilation effectiveness in a room with floor/ceiling heating and mixing/displacement ventilation, Proceedings of the 8th international symposium on heating, ventilation and air conditioning, Springer, 2014, pp. 59-67.
[29] Z. Lin, T. Chow, C. Tsang, Stratum ventilation? A conceptual introduction, Proceedings of the 10th international conference on indoor air quality and climate (2005).
[30] H. Li, C. Xi, X. Kong, Z. Lin, L. Wang, A comparative experimental investigation on radiant floor heating system and stratum ventilation, Sustain. Cities Soc. 52 (2020).
[31] J. Lyu, X. Feng, Y. Cheng, C. Liao, Experimental and numerical analysis of air temperature uniformity in occupied zone under stratum ventilation for heating mode, J. Build. Eng. 43 (2021).
[32] J. Liu, Z. Lin, Energy and exergy analyze of different air distributions in a residential building, Energy Build. 233 (2021).
[33] X. Kong, C. Xi, H. Li, Z. Lin, A comparative experimental study on the performance of mixing ventilation and stratum ventilation for space heating, Build. Environ. 157 (2019) 34–46.
[34] Z. Lin, C.K. Lee, S. Fong, T.T. Chow, T. Yao, A. Chan, Comparison of annual energy performances with different ventilation methods for cooling, Energy Build. 43 (1) (2011) 130–136.
[35] S. Liang, W. Wang, Y. Sun, Z. Li, J. Zhao, Y. Lin, S. Deng, A novel design method for ASHPs considering output heating capacity and frosting suppression, Energy Build. 224 (2020).
[36] D. Osborne, The Coal Handbook: Towards Cleaner Production: Volume 2: Coal Utilisation, Elsevier2013.
[37] Q. Zhang, L. Zhang, J. Nie, Y.J.A.E. Li, Techno-economic analysis of air source heat pump applied for space heating in northern China, Appl. Energy 207 (2017) 533–542.
[38] G. Angrisani, F. Minichiello, M. Sasso, Improvements of an unconventional desiccant air conditioning system based on experimental investigations, Energy Convers. Manage. 112 (2016) 423–434.
[39] M. Ghazikhani, I. Khazaee, S. Vahidifar, Exergy analysis of two humidification process methods in air-conditioning systems, Energy Build. 124 (2016) 129–140.
[40] H. Li, W.L. Lee, J. Jia, Applying a novel extra-low temperature dedicated outdoor air system in office buildings for energy efficiency and thermal comfort, Energy Convers. Manage. 121 (2016) 162–173.
[41] J. Léger, D.R. Rousse, K. Le Borgne, S. Lassue, Comparing electric heating systems at equal thermal comfort: an experimental investigation, Build. Environ. 128 (2018) 161–169.
[42] L. Li, Y. Fu, J.C. Fung, H. Qu, A.K. Lau, Development of a back-propagation neural network and adaptive grey wolf optimizer algorithm for thermal comfort and energy consumption prediction and optimization, Energy Build. 253 (2021).
[43] H. Parhizkar, R.A. Khoraskani, M. Tahbaz, Double skin façade with Azolla; ventilation, indoor air quality and thermal performance assessment, J. Cleaner Prod. 249 (2020).
[44] C. Li, H. Tang, Comparison of COVID-19 infection risks through aerosol transmission in supermarkets and small shops, Sustain. Cities Soc. 76 (2022).
[45] J. Tang, C. Noakes, P.V. Nielsen, I. Eames, A. Nicolle, Y. Li, G. Settles, Observing and quantifying airflows in the infection control of aerosol-and airborne-transmitted diseases: an overview of approaches, J. Hosp. Infect. 77 (3) (2011) 213–222.
[46] W. Wu, Z. Lin, Experimental study of the influence of a moving manikin on temperature profile and carbon dioxide distribution under three air distribution methods, Build. Environ. 87 (2015) 142–153.
[47] Z. Wang, Y. Hu, J. Jiang, Numerical investigation of leaking and dispersion of carbon dioxide indoor under ventilation condition, Energy Build. 66 (2013) 461–466.
[48] I. Iso, 7730: Ergonomics of the thermal environment Analytical determination and interpretation of thermal comfort using calculation of the PMV and PPD indices and local thermal comfort criteria, Management 3 (605) (2005) e615.
[49] Z. Lin, Effective draft temperature for evaluating the performance of stratum ventilation, Build. Environ. 46 (9) (2011) 1843–1850.
[50] T. Li, Y. Jia, J. Wang, N. Meng, Q. Liu, H. Qin, Energy, economic and environmental evaluation of a novel combined cooling and power system characterized by temperature and humidity independent control, Energy Convers. Manage. 215 (2020).
[51] G. Cao, P. Nielsen, R. Jensen, P. Heiselberg, L. Liu, J. Heikkinen, Protected zone ventilation and reduced personal exposure to airborne cross-infection, Indoor Air 25 (3) (2015) 307–319.
[52] I.S.o.t.P.s.R.o. China, echnical specification for radiant heating and cooling (JGJ 142-2012), 2012.
[53] G. Lidén, J. Waher, Experimental investigation of the concept of a 'breathing zone'using a mannequin exposed to a point source of inertial/sedimenting particles emitted with momentum, Ann. Occup. Hyg. 54 (1) (2010) 100–116.
[54] ASHRAE, ASHRAE Standard 55–2017 Thermal environmental conditions for human occupancy, ASHRAE, 2017.
[55] A.K. Persily, Ventilation effectiveness in mechanically ventilated office buildings, US Department of Commerce, National Bureau of Standards1985.
[56] J. Ling, H. Tong, J. Xing, Y. Zhao, Simulation and optimization of the operation strategy of ASHP heating system: a case study in Tianjin, Energy Build. 226 (2020).
[57] I. Olmedo, P.V. Nielsen, M. Ruiz de Adana, R.L. Jensen, The risk of airborne cross-infection in a room with vertical low-velocity ventilation, Indoor Air 23 (1) (2013) 62–73.
[58] C. Sun, Z. Zhai, The efficacy of social distance and ventilation effectiveness in preventing COVID-19 transmission, Sustain. Cities Soc. 62 (2020).
[59] P. Azimi, B. Stephens, HVAC filtration for controlling infectious airborne disease transmission in indoor environments: predicting risk reductions and operational costs, Build. Environ. 70 (2013) 150–160.
[60] N. Meng, T. Li, J. Wang, Y. Jia, Q. Liu, H.J.R.E. Qin, Synergetic mechanism of fracture properties and system configuration on techno-economic performance of enhanced geothermal system for power generation during life cycle, 152 (2020) 910-924.
[61] A. Aganovic, M. Steffensen, G. Cao, CFD study of the air distribution and occupant draught sensation in a patient ward equipped with protected zone ventilation, Build. Environ. 162 (2019).